Article

Atomistic Molecular Dynamics Simulations of Chemical Force Microscopy

David L. Patrick, Flanagan, Patrick Kohl, and Ruth M. Lynden-Bell

J. Am. Chem. Soc., **2003**, 125 (22), 6762-6773• DOI: 10.1021/ja0345367 • Publication Date (Web): 10 May 2003

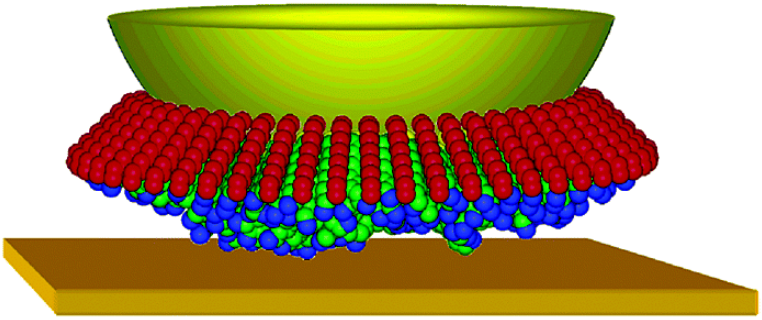

J|A|C|S
ARTICLES
Published on Web 05/10/2003

Atomistic Molecular Dynamics Simulations of Chemical Force Microscopy

David L. Patrick,*,† John F. Flanagan, IV,† Patrick Kohl,† and Ruth M. Lynden-Bell‡

Contribution from the Department of Chemistry, Western Washington University, 516 High Street, Bellingham, Washington 98225 and Atomistic Simulation Group, School of Mathematics and Physics, The Queen's University of Belfast, Belfast BT7 1NN, Northern Ireland, U.K.

Received February 6, 2003; E-mail: patrick@chem.wwu.edu

Abstract: Chemical force microscopy and related force measurement techniques have emerged as powerful tools for studying fundamental interactions central to understanding adhesion and tribology at the molecular scale. However, detailed interpretation of these interactions requires knowledge of chemical and physical processes occurring in the region of the tip−sample junction that experiments cannot provide, such as atomic-scale motions and distribution of forces. In an effort to address some of these open issues, atomistic molecular dynamics simulations were performed modeling a chemical force microscope stylus covered with a planar C12 alkylthiolate self-assembled monolayer (SAM) interacting with a solid wall. A complete loading−unloading sequence was simulated under conditions of near-constant equilibrium, approximating the case of infinitely slow tip motion. In the absence of the solid wall, the stylus film existed in a fluid state with structural and dynamic properties similar to those of the analogous planar SAM at an elevated temperature. When the wall was brought into contact with the stylus and pressed against it, a series of reversible changes occurred culminating with solidification of the SAM film at the largest compressive force. During loading, the chemical composition of the contact changed, as much of the film's interior was exposed to the wall. At all tip heights, the distribution of forces within the contact zone was uneven and subject to large local fluctuations. Analysis using the Johnson−Kendall−Roberts, Derjaguin−Muller−Toporov, and Hertz contacts mechanics models revealed significant deviations from the simulation results, with the JKR model providing best overall agreement. Some of the discrepancies found would be overlooked in an actual experiment, where, unlike the simulations, contact area is not separately known, possibly producing a misleading or incorrect interpretation of experimental results. These shortcomings may be improved upon by using a model that correctly accounts for the finite thickness of the compliant components and nonlinear elastic effects.

Introduction

In the science of adhesion and tribology, one of the most fundamental and important pairings is that between a small asperity and a flat surface. Macroscopic adhesive and tribological phenomena ultimately originate with the microscopic properties of contacting surfaces, and the asperity-flat pairing is considered a model for the microscopic geometry occurring in most cases of technological relevance.[1] While the importance of single asperity contacts has been recognized for many decades, their direct experimental study accelerated dramatically with the invention of the atomic force microscope[2] (AFM), which enables controlled measurements involving asperity-flat pairings at nanometer-length scales and nanonewton forces. However, for quantitative measurements, one shortcoming of AFM is that the chemical and physical characteristics of the asperity are generally not well defined or controlled, especially when an experiment is performed under ambient conditions or in solution.[3] Aside from adjusting the bulk solution environment (e.g., pH), there is no practical way to control the chemistry of the probe or to prevent the formation of a contamination layer.

Chemical force microscopy (CFM) is a variation of AFM which solves some of these problems by employing a stylus coated with a self-assembled monolayer (SAM) of chainlike molecules.[4] CFM provides a way to tailor the properties of the probe through chemical derivatization of the terminal group and chain, enabling measurement of chemically specific interactions between a small number of stylus and sample molecules with high spatial and force resolution. When compared to force measurements made using conventional unmodified tips, CFM therefore involves relatively well-controlled conditions. The technique has been used to map chemically distinct surface domains,[5] to quantitatively measure friction[6] and adhesion[7] forces for a variety of probe and surface chemical pairings, and to investigate the effect of different solvents[8] and solvent pH

† Western Washington University.
‡ The Queen's University of Belfast.

(1) Bowden, F. P.; Tabor, D. *The Friction and Lubrication of Solids*; Clarendon Press: Oxford, 1985.
(2) Binning, G.; Quate, C. F.; Gerber, Ch. *Phys. Rev. Lett.* **1986**, *56*, 930.
(3) Iler, R. K. *The Chemistry of Silica*; Wiley-Interscience: New York, 1979.
(4) Frisbie, C. D.; Rozsnyai, L. F.; Noy, A.; Wrighton, M. S.; Lieber, C. M. *Science* **1994**, *265*, 2071.

 10.1021/ja0345367 CCC: $25.00

values[9] on measured interaction forces. Very complex interactions, such as DNA base pairings and discrimination on the basis of molecular chirality are also possible.[10] CFM is reviewed in ref 11.

Detailed interpretation of chemical interactions in scanning probe microscopy ultimately requires an atomic-level understanding of the chemical and physical processes occurring in the region of the tip−sample junction.[12] However, the forces measured in scanning probe measurements represent the cumulative effect of multiple simultaneous interactions involving many atoms, averaged over a characteristic measurement time which is generally much longer than the time scale associated with atomic and molecular motions. In fact, it appears that many, if not most, AFM and CFM experiments actually involve multiple asperity contacts due to the nanometer-scale roughness of the stylus and surface.[13] In CFM, molecular order and dynamics in the SAM coating will also play important roles. There are indications that alkylsilane SAMs grafted onto Si_3N_4 tips exist in a relatively disordered and fluid state compared to SAMs on planar substrates, but few details are known.[14] The appropriateness of the most widely used models of contact mechanics for describing force microscopy and nanometer-sized contacts also has yet to be firmly established. A variety of results have shown that the stylus−surface interaction can be dominated by discrete events, in some cases, allowing measurement of individual bond-rupture forces.[15,16] Continuum models will not perform well under such conditions. AFM tips as sharp as $R <$ 10 nm are now commercially available, which may be sharp enough to produce a single molecular pair contact at rupture.[9]

Atomistic computer modeling is a potentially powerful tool for investigating many of these issues. Previous studies include analytical models describing tip−sample interactions,[17] scanning motion,[18] and image formation;[19] static calculations[20] or atomistic simulations based on energy minimization[21] or molecular dynamics[22] using empirical potentials; and investigations which take explicit account of electronic effects and chemical bond formation through semiempirical[23] or ab initio[24] methods. Many of the earlier findings are reviewed in ref 25. A smaller number of molecular dynamics and Monte Carlo simulations have examined the case of planar SAMs compressed by a planar wall or indented by a sharp stylus;[26] however, the important geometry represented in CFM, that of a curved SAM on a sharp stylus interacting with a planar wall, has so far received very little attention.[27]

The goal of this work was to perform realistic, atomic-scale simulations of CFM in order to address questions left unanswered by experiments. A model was investigated representing a sharp stylus covered by a uniform alkylthiolate SAM interacting with a smooth, planar wall. The simulations were performed under conditions of pseudoconstant equilibrium using small stepwise displacements in tip height. We report on the arrangement and dynamics of molecules on the stylus, the origin, nature, and spatial distribution of interaction forces, and changes occurring as a result of interactions with the planar wall. The contact area, force, and indentation were measured and are analyzed within the framework of several popular models of contact mechanics, and differences with the simulation results are explained in terms of specific, atomic-level phenomena. In addition to providing the most detailed description yet of fundamental processes and interactions occurring in CFM and related techniques, we have obtained several surprising findings which alter our understanding of the proper way to approach interpretation of experimental measurements.

Model

The CFM stylus was modeled as a 10 nm diameter gold sphere, partially covered with a compact monolayer of dode-

(5) (a) Green, J.-B. D.; McDermott, M. T.; Porter, M. D. *J. Phys. Chem*. **1995**, *99*, 10960. (b) Akari, S.; Horn, D.; Kellar, H.; Schrepp, W. *Adv. Mater*. **1995**, *7*, 549. (c) Heaton, M. G.; Prater, C. B.; Kjoller, K. J. *Adv. Mater. Processes* **1996**, *149*, 27.

(6) (a) Noy, A.; Frisbie, C. D.; Rozsnyai, L. F.; Wrighton, M. S.; Lieber, C. M. *J. Am. Chem. Soc*. **1995**, *117*, 7943. (b) Akari, S.; Schrepp, W.; Horn, D. *Ber. Bunsen-Ges*. **1996**, *100*, 1014. (c) McDermott, M. T.; Green, J.-B. D.; Porter, M. D. *Langmuir* **1997**, *13*, 2504. (d) Meyer, E.; Overney, R.; Brodbeck, D.; Howald, L.; Luthi, R.; Frommer, J.; Guntherodt, H.-J. *Phys. Rev. Lett*. **1992**, *69*, 1777.

(7) (a) Han, T.; Williams, J. M.; Beebe, T. P., Jr. *Analytica Chim. Acta* **1995**, *307*, 365. (b) Williams, J. M.; Han, T.; Beebe T. P., Jr. *Langmuir* **1996**, *12*, 1291. (c) Wenzler, L. A.; Moyes, G. L.; Olson, L. G.; Harris, J. M.; Beebe, T. P., Jr. *Anal. Chem*. **1997**, *69*, 2855. (d) Wenzler, L. A.; Moyes, G. L.; Raikar, G. N.; Hansen, R. L.; Harris, J. M.; Beebe, T. P., Jr.; Wood, L.; Saavedra, S. S. *Langmuir* **1997**, *13*, 3761. (e) van der Vegte, E. W.; Hadziioannou, G. *Langmuir* **1997**, *13*, 4357.

(8) Sinniah, S. K.; Steel, A. B.; Miller, C. J.; Reutt-Robey, J. E. *J. Am. Chem. Soc*. **1996**, *118*, 8925.

(9) (a) Vezenov, D. V.; Noy, A.; Rozsnyai, L. F.; Lieber, C. M. *J. Am. Chem. Soc*. **1997**, *119*, 2006. (b) Ashby, P. D.; Chen. L.; Lieber, C. M. *J. Am. Chem. Soc*. **2000**, *122*, 9467.

(10) McKendry, R.; Theoclitou, M.-E.; Rayment, T.; Abell, C. *Nature* **1998**, *391*, 566.

(11) Noy, A.; Vezenov, D. V.; Lieber, C. M. *Annu. Rev. Mater. Sci*. **1997**, *27*, 381.

(12) Carpick, R. W.; Salmeron, M. *Chem. Rev*. **1997**, *97*, 1163.

(13) (a) Sheiko, S. S.; Moller, M.; Reuvekamp, E. M. C. M.; Zandbergen, H. W. *Ultramicroscopy* **1994**, *53*, 371. (b) Xu, S.; Arnsdorf, M. F. *J. Microsc. (Oxford)* **1994**, *173*, 199.

(14) Ito, T.; Madoka, N.; Bühlmann, P.; Umezawa, Y. *Langmuir* **1997**, *13*, 4323.

(15) (a) Hoh, J. H.; Cleveland, J. P.; Prater, C. B.; Revel, J.-P.; Hansma, P. K., *J. Am. Chem. Soc*. **1992**, *114*, 4917. (b) Skulason, H.; Frisbie, C. D. *J. Am. Chem. Soc*. **2002**, *124*, 15125.

(16) Skulason, H.; Frisbie, C. D. *Anal. Chem*. **2002**, *74*, 3096.

(17) (a) Goodman, F. O.; Garcia, N. *Phys. Rev. B* **1991**, *43*, 4728. (b) Hartmann, U. *Phys. Rev. B* **1991**, *43*, 2404.

(18) Tomanek, D.; Zhong, W.; Thomas, H. *Europhys. Lett.* **1991**, *15*, 887.

(19) Sokolov, I. Y. *Surf. Sci*. **1994**, *311*, 287.

(20) Abraham, F. F.; Batra, I. P.; Ciraci, S. *Phys. Rev. Lett.* **1988**, *60*, 1314.

(21) (a) Sasaki, N.; Tsukada, M. *Jpn. J. Appl. Phys., Part 1* **1995**, *34*, 3319. (b) Xu, L.; Yao, X.-W.; Zhang, L.-P.; Li, M.-Q.; Yang, F.-J. *Phys. Rev. B* **1995**, *51*, 10013. (c) Tang, H.; Joachim, C.; Devillers, J. *Surf. Sci*. **1993**, *291*, 439. (d) Gould, S. A. C.; Burke, K.; Hansma, P. K. *Phys. Rev. B* **1989**, *40*, 5363. (e) Abraham, F. F.; Batra, I. P. *Surf. Sci. Lett*. **1989**, *209*, L125.

(22) (a) Sumpter, B. G.; Getino, C.; Noid, D. W.; Wunderlich, B. *Makromol. Chem., Theory Simul*. **1993**, *2*, 55. (b) Rafii-Tabar, H.; Pethica, J. B.; Sutton, A. P. *Mater. Res. Soc. Symp. Proc*. **1992**, *239*, 313. (c) Sutton, A. P.; Pethica, J. B. *J. Phys.: Condens. Matter* **1990**, *2*, 5317. (d) Landman, U.; Harrison, J. A.; White, C. T.; Colton, R. J.; Brenner, D. W. *Surf. Sci*. **1992**, *271*, 57. (e) Shluger, A. L.; Wilson, R. M.; Williams, R. T. *Phys. Rev. B* **1994**, *49*, 4915. (f) Tsujimishi, K.; Tamura, H.; Hirotani, A.; Kubo, M.; Komiyama, M.; Miyamoto, A. *J. Phys. Chem. B* **1997**, *101*, 4260. (g) Jung, T. A.; Schlittler, R. R.; Gimzewski, J. K.; Tang, H.; Joachim, C. *Science* **1996**, *271*, 181. (h) Sinnott, S. B.; Colton, R. J.; White, C. T.; Brenner, D. W. *Surf. Sci. Lett*. **1994**, *316*, L1055. (i) Harrison, J. A.; White, C. T.; Colton, R. J.; Brenner, D. W. *Thin Solid Films* **1995**, *260*, 205. (j) Landman, U.; Luedtke, W. D. *J. Vac. Sci. Technol*. **1991**, *B9*, 414. (k) Sumpter, B. G.; Getino, C.; Noid, D. W. *J. Chem. Phys*. **1992**, *96*, 7072. (l) Harrison, J. A.; White, C. T.; Colton, R. J.; Brenner, D. W. *Phys. Rev. B* **1992**, *46*, 9700.

(23) (a) Ness, H.; Gautier, F. *J. Phys.: Condens. Matter* **1995**, *7*, 6625. (b) Ness, H.; Gautier, F. *J. Phys.: Condens. Matter* **1995**, *7*, 6641. (c) Komiyama, M.; Tsujmishi, K.; Ohkubo, S.; Tazawa, K.; Kubo, M.; Miyamoto, A. *Jpn. J. Appl. Phys., Part 2* **1995**, *34*, L789. (d) Shluger, A. L.; Rohl, A. L.; Wilson, R. M.; Williams, R. T. *J. Vac. Sci. Technol*. **1995**, *B13*, 1155.

(24) Ciraci, S.; Baratoff, A.; Batra, I. P. *Phys. Rev. B* **1990**, *41*, 2763.

(25) Harrison, J. A.; Brenner, D. W. In *The Handbook of Micro/Nano Tribology*; Bhushan, B., Ed.; CRC Press: Boca Raton, FL, 1995.

(26) (a) Leng, Y. S.; Jiang, S. *J. Chem. Phys.* **2000**, *113*, 8800. (b) Siepmann, J. I.; McDonald, I. R., *Phys. Rev. Lett*. **1993**, *70*, 453. (c) Karaborni, S. *Phys. Rev. Lett* **1994**, *73*, 1668. (d) Glosli, J. N.; McClelland, G. M. *Phys. Rev. Lett*. **1993**, *70*, 1960. (e) Tupper, K. J.; Colton, R. J.; Brenner, D. W. *Langmuir* **1994**, *10*, 2041. (f) Callaway, M.; Tildesley, D. J.; Quirke, N. *Langmuir* **1994**, *10*, 3350. (g) Bonner, T.; Baratoff, A. *Surf. Sci*. **1997**, *377−379*, 1082.

(27) Leng, Y.; Jiang, S. *J. Am. Chem. Soc*. **2002**, *124*, 11764.

Table 1. Force Field Parameters and Potential Functions

	bond stretching	r is the bond length.
$U_{bond} = (1/2)k(r - r_0)^2$	$k_{S-CH_2} = 3.20 \times 10^{-16}$ J nm^{-2}	$r_0(S-CH_2) = 0.1815$ nm
	$k_{CH_2-CH_2} = 4.39 \times 10^{-16}$ J nm^{-2}	$r_0(CH_2-CH_2) = 0.1523$ nm
	$k_{CH_2-CH_3} = 4.39 \times 10^{-16}$ J nm^{-2}	$r_0(CH_2-CH_3) = 0.1523$ nm
	angle bending	θ is the bond angle.
$U_{angle} = (1/2)k(\theta - \theta_0)^2$	$k_{S-CH_2-CH_2} = 8.629 \times 10^{-19}$ J rad^{-2}	$\theta_0(S-CH_2-CH_2) = 1.997$ rad
	$k_{CH_2-CH_2-CH_2} = 8.629 \times 10^{-19}$ J rad^{-2}	$\theta_0(CH_2-CH_2-CH_2) = 1.911$ rad
	$k_{CH_2-CH_2-CH_3} = 8.629 \times 10^{-19}$ J rad^{-2}	$\theta_0(CH_2-CH_2-CH_3) = 1.911$ rad
	bond torsion	ϕ is the dihedral angle.
$U_{torsion} = \sum_{i=0}^{5} a_i \cos^i(\phi)$	$a_0 = 1.54 \times 10^{-20}$ J	
	$a_1 = 2.02 \times 10^{-20}$ J	
	$a_2 = -2.18 \times 10^{-20}$ J	
	$a_3 = -5.08 \times 10^{-21}$ J	
	$a_4 = 4.36 \times 10^{-20}$ J	
	$a_5 = -5.23 \times 10^{-20}$ J	
	nonbonded interactions	r is the interatomic separation.
$U_{LJ} = 4\epsilon[(\sigma/r)^{12} - (\sigma/r)^6]$	$\epsilon_{S-S} = 2.761 \times 10^{-21}$ J	$\sigma_{S-S} = 0.425$ nm
	$\epsilon_{S-CH_2} = 1.194 \times 10^{-21}$ J	$\sigma_{S-CH_2} = 0.372$ nm
	$\epsilon_{S-CH_3} = 1.455 \times 10^{-21}$ J	$\sigma_{S-CH_3} = 0.372$ nm
	$\epsilon_{CH_2-CH_2} = 8.202 \times 10^{-22}$ J	$\sigma_{CH_2-CH_2} = 0.3905$ nm
	$\epsilon_{CH_2-CH_3} = 9.988 \times 10^{-22}$ J	$\sigma_{CH_2-CH_3} = 0.3905$ nm
	$\epsilon_{CH_3-CH_3} = 1.216 \times 10^{-21}$ J	$\sigma_{CH_3-CH_3} = 0.3905$ nm
	stylus core and wall potential	z is the distance between an atom and the stylus core or wall.
$U_{wall} = C_{12}/(z - z_0)^{12} - C_3/(z - z_0)^3$	$C_3(S) = 2.49 \times 10^{-21}$ J nm^3	$z_0(S) = 0.0269$ nm
	$C_3(CH_2) = 2.36 \times 10^{-22}$ J nm^3	$z_0(CH_2) = 0.086$ nm
	$C_3(CH_3) = 2.87 \times 10^{-22}$ J/nm^3	$z_0(CH_3) = 0.086$ nm
	$C_{12}(S) = 5.65 \times 10^{-28}$ J nm^{12}	
	$C_{12}(CH_2) = 3.87 \times 10^{-28}$ J nm^{12}	
	$C_{12}(CH_3) = 4.71 \times 10^{-28}$ J/nm^{12}	
	sulfur atom tethering	r is the distance between a sulfur atom and its tethering point.
$U_{tethering} = (1/2)kr^2$	$k = 1.89 \times 10^{-16}$ J nm^{-2}	

canethiolate ($S(CH_2)_{11}CH_3$). The choice of a spherical shape for the stylus core was motivated by two considerations. First, the actual atomic-level shape of the very end of a CFM stylus (or corresponding asperity in other nanotribology measurements) is almost never known, is different from stylus to stylus, and may change over the course of repeated measurements. Any particular choice of atomic-scale stylus shape is therefore arbitrary. Second, a spherical stylus facilitates the drawing of general conclusions by revealing generic phenomena more easily recognized and analyzed using a simplified geometry. It should be noted however that the smoothly curved shape of the stylus modeled here is different from that of a real metal nanoparticle, which would be highly faceted, leading to interactions which would depend on orientation as well as size. Because the model stylus lacked flat facets, there were no regular, terrace-like adsorption sites to promote formation of ordered regions in the SAM. Consequently, the film modeled here was less well-ordered than experimental and computational studies have found SAMs on planar surfaces and actual metal nanoparticles to be.[28−30]

The molecules and their interactions with the tip core and planar sample surface were treated using the model presented in Table 1. It is a modification of Model 1 in ref 31 in which CH_2 and CH_3 groups are treated as integrated pseudoatoms. Bond stretching was modeled with a harmonic potential to allow for compression-induced bond length changes.[32] Dihedral distortions were represented using the cosine sum potential of Ryckaert and Bellemans.[33] Interatomic interactions were treated using the Lennard−Jones potential, which was applied to all pairs of atoms on different molecules and to all pairs of atoms within the same molecule separated by at least three skeletal bonds. Nonbonded interactions were truncated at 1.2 nm.

The use of a model developed for planar SAMs on the curved surface of the tip appears appropriate because three-dimensional SAMs are similar in many respects to their planar counterparts. For example, dodecylthiolate films on gold nanoparticles larger than 4−5 nm in diameter exhibit properties such as thiol coverage and concentration of gauche bonds in the chain backbones that are essentially the same as those for planar SAMs.[34] Even on particles as small as 1 nm in diameter, infrared and Raman spectroscopic measurements show long-chained alkylthiolate SAMs can form of highly crystalline films with few gauche bonds, comparable to planar SAMs,[35] and the chain-length dependence of order−disorder transition temperatures of

(28) (a) Brust, M.; Fink, J.; Bethell, D.; Schiffrin, D. J.; Kiely, C. J. *J. Chem. Soc., Chem. Commun.* **1995**, 1655. (b) Badia, A.; Gao, W.; Singh, S.; Demers, L.; Cuccia, L.; Reven, L. *Langmuir* **1996**, *12*, 1262. (c) Badia, A.; Singh, S.; Demers, L.; Cuccia, L.; Brown, G. R.; Lennox, R. B. *Chem.—Eur. J.* **1996**, *2*, 359. (d) Terrill, R. H.; Postlethwaite, T. A.; Chen, C.-H.; Poon, C.-D.; Terzis, A.; Chen, A.; Hutchison, J. E.; Clark, M. R.; Wignall, G.; Londono, J. D.; Superfine, R.; Falvo, M.; Johnson, C. S., Jr.; Samulski, E. T.; Murray, R. W. *J. Am. Chem. Soc.* **1995**, *117*, 12537. (e) Brust, M.; Fink, J.; Bethell, D.; Schiffrin, D. J.; Kiely, C. J. *J. Chem. Soc., Chem. Commun.* **1995**, 1655.
(29) Hostetler, M. J.; Stokes, J. J.; Murray R. W. *Langmuir* **1996**, *12*, 3604.
(30) Luedtke, W. D.; Landman, U. *J. Phys. Chem.* **1996**, *100*, 13323.
(31) Hautman, J.; Klein, M. L. *J. Chem. Phys.* **1989**, *91*, 4994.
(32) Tupper, K. J.; Brenner, D. W. *Langmuir* **1994**, *10*, 2335.
(33) Ryckaert, J. P.; Bellemans, A. *J. Chem. Soc., Faraday Discuss.* **1978**, *66*, 95.
(34) Hostetler, M. J.; Wingate, J. E.; Zhong, C.-J.; Harris, J. E.; Vachet, R. W.; Clark, M. R.; Londono, J. D.; Green, S. J.; Stokes, J. J.; Wignall, G. D.; Glish, G. L.; Porter, M. D.; Evans, N. D.; Murray, R. W. *Langmuir* **1998**, *14*, 17.
(35) Porter, L. A., Jr.; Ji, D.; Westcott, S. L.; Graupe, M.; Czernuszewicz, R. S.; Halas, N. J.; Lee, T. R. *Langmuir* **1998**, *14*, 7378.

SAMs on nanoparticles show similar trends to planar SAMs.[36] X-ray photoelectron spectroscopy, nuclear magnetic resonance spectroscopy, and infrared spectroscopy all indicate that the thiolate−gold bond is the same on gold nanoparticles as it is on planar gold substrates.[37]

The performance of united atom models in describing planar SAMs is also well documented.[38] They generally reproduce the chain tilt angle, gauche bond distribution, and gross phase behavior but fail to reproduce experimentally observed chain packing and superstructures.[39] Molecular mechanics force fields appear able to predict the Young's moduli of planar SAMs to within about a factor of 2.[40] Less is known about the performance of united atom models in describing nonplanar SAMs, but MD simulations of alkylthiolate films on 1−2 nm diameter gold nanoparticles do predict properties in qualitative agreement with experiment.[30]

Both the planar wall and CFM stylus core were modeled as perfectly smooth (nonatomistic) solids interacting with chain psuedoatoms through a 12−3 function with parameters for gold. The stylus core and planar wall did not interact with one another. Note that the perfect smoothness of the substrate meant that when it was brought into contact with the stylus film, shear stresses could not be sustained; that is, the contact was frictionless. Sulfur atoms adsorbed to the tip core were prevented from moving across the surface of the sphere by a harmonic tethering potential which depended only on a sulfur atom's position relative to its tethering point. The spring constant for the tethering potential was obtained by fitting the bottom of the 12−3 potential used for the radial interaction. No cutoff was applied to the wall potentials.

Simulations were performed using a modified version of the parallel molecular dynamics program DL-POLY.[41] The temperature was held at 300 K using a Berendsen thermostat with a time constant of 0.1 ps applied to all atoms, which produced a root-mean-squared fluctuation in temperature of 3 K. Newton's equations of motion were integrated using the Verlet leapfrog algorithm with a time step of 1×10^{-15} s.

The system was prepared by covering the bottom portion of the spherical tip with 278 chains arranged in equally spaced rings, with the chain backbones directed radially outward (the backbone was defined as the line joining the 1st, 3rd, 5th, ..., 13th psuedoatoms). The film density at the surface of the tip core was 0.216 nm^2 per chain, close to the density adopted by alkylthiolate SAMs on a planar gold surfaces (0.217 nm^2).[42] Farthest up the side of the tip, a ring of 52 molecules was frozen in place for the duration of the simulations, acting as a confining "skirt" to prevent the dynamic molecules from splaying out toward or migrating onto the upper portion of the tip. Some other effects of this skirt are discussed below. The film thickness

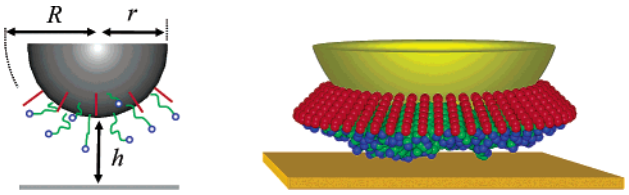

Figure 1. Stylus consisted of a smooth sphere covered on its lower portion by a uniform self-assembled monolayer (SAM) of 278 dodecylthiolate chains. The spherical core had a radius $r = 5.0$ nm and interacted with SAM molecules with a potential modeling gold. Alkylthiolate molecules were prevented from moving across the surface of the sphere through a tethering potential applied to each sulfur atom and prevented from splaying upward by a rigidly fixed encircling alkylthiolate skirt. In the absence of the planar wall, the thickness of the SAM film averaged 1.53 nm, giving an effective stylus radius of $R = 6.53$ nm. Throughout the text, the stylus height h is measured, as shown in the figure, as the distance from the bottom of the tip core to the planar wall. Methyl psuedoatoms are colored blue, methylene psuedoatoms are green, and frozen molecules are red.

for the isolated tip was 1.53 nm (calculated as the average distance between terminal CH_3 groups and the sphere surface), which was ∼10% thinner than a planar alkylthiolate SAM of the same chain length. A schematic diagram of the stylus is shown in Figure 1.

After molecules were placed on the tip, the potential energy of the system was minimized, followed by 450 ps of simulation at 300 K. During this process, the planar gold wall was removed from the system, and the sulfur atom tethering potential was turned off, freeing the chains to migrate about the lower portion of the tip. At the end of the equilibration period, when the potential energy of the system was constant, tethers were applied, restraining the sulfur atoms from long-distance motion. The tethering energy was always less than 1% of the total potential energy, even when the film was pressed strongly against the planar wall.

After the stylus was prepared in isolation, it was placed $h = 2.04$ nm above the planar surface, where h is defined as the spacing between the planar wall and the surface of the spherical stylus core, as shown in Figure 1. At this height, the terminal alkylthiolate methyl groups at the bottom of the tip were 0.5 nm above the planar wall. The wall was then gradually raised to $h = 0.76$ nm, bringing it into contact with the stylus, and lowered again, returning to its initial position. Throughout this process, the shapes of the planar wall and stylus core were kept unchanged; only the SAM film covering the stylus was allowed to deform. As will be shown in the following, the film is roughly an order of magnitude more compliant than gold, so the approximation of a rigid wall and sphere is a good one so long as the loading is not too great.

The behavior of this system was found to be very sensitive to the speed at which the tip was moved because the film underwent complex, slow relaxation dynamics. In simulations where the wall was moved in continuous motion, the force curve displayed large hysteresis. Mechanical indentation measurements on Langmuir−Blodgett films[43] and SAMs[44] also show time-dependent responses in the films, indicating rearrangement processes among film molecules which can be irreversible or slow to recover on the time scale of the experiments. In a CFM

(36) Badia, A.; Cuccia, L.; Demers, L.; Morin, F. G.; Lennox, R. B. *J. Am. Chem. Soc.* **1997**, *119*9, 2682.
(37) (a) Castner, D. G.; Hinds, K.; Grainger, D. W. *Langmuir* **1996**, *12*, 5083. (b) Badia, A.; Demers, L.; Dickinson, L.; Morin, F. G.; Lennox, R. B.; Reven, L. *J. Am. Chem. Soc.* **1997**, *119*, 11104.
(38) Siepmann, J. I.; McDonald, I. R. *Langmuir* **1993**, *9*, 2351.
(39) (a) Camillone N., III.; Chidsey, C. D. D.; Eisenberger, P.; Fenter, P.; Li, J.; Liang, K. S.; Liu, G.-Y.; Scoles, G. *J. Chem. Phys.* **1993**, *99*, 744. (b) Anselmetti, D.; Baratoff, A.; Güntherodt, H.-J.; Delamarche, E.; Michel, B.; Gerber, Ch.; Kang, H.; Wolf, H.; Ringsdorf, H. *Europhys. Lett.* **1994**, *27*, 365.
(40) Henda, R.; Grunze, M.; Pertsin, A. J. *Tribol. Lett.* **1998**, *5*, 191.
(41) Forester, T. R. Daresbury Laboratory: Warrington WA4 4AD, United Kingdom.
(42) Dubois, L. H.; Nuzzo, R. G. *Annu. Rev. Phys. Chem.* **1992**, *43*, 437.
(43) (a) Chen, Y. L.; Helm, C. A.; Israelachvili, J. N. *J. Phys. Chem.* **1991**, *95*, 10736. (b) Joyce, S. R.; Michalske, R. A.; Crooks, R. M. *Phys. Rev. Lett.* **1992**, *68*, 2790.
(44) Blackman, G. S.; Mate, C. M.; Philpott, M. R. *Phys. Rev. Lett.* **1990**, *65*, 2270.

experiment measuring force−height relationships, the tip is typically lowered and raised at an average speed of $\sim 10^{-6}$ m s^{-1}, which is several orders of magnitude slower than it is feasible to simulate.

In this study, we examined a limiting case approximating infinitely slow tip motion by equilibrating the system at 24 different heights (half during loading and half during unloading), where the initial configurations were taken from a simulation of continuous motion in which the wall was moved at 2 ms^{-1}. At each of the 24 chosen tip heights, the system was simulated until all parameters had reached steady-state values, which required 1−2 ns per point. This was followed by an additional 1−1.5 ns of simulation during which various parameters were measured and tabulated. This is still a short time scale compared with the rate of tip motion used in most experiments, where the stylus position typically changes by only $\sim 10^{-6}$ nm in 1 ns. Nevertheless, all indications pointed to the system remaining at or near equilibrium at each tip position.

The system modeled an apparatus of the type in which it is the displacement between the stylus and sample, rather than the force between them, that is controlled. Thus, unlike, for example, the AFM or surface forces apparatus,[45] where one component is attached to a flexible spring, the stylus here was held rigidly fixed at each height. In this respect, the model was expected to behave similarly to the interfacial force microscope invented by Houston, Michalske, and co-workers,[46] where displacement is controlled via electrostatic forces, or to the method used by Pethica and co-workers[47] involving control with magnetic forces.

To judge the effects of the frozen skirt, we performed simulations at several tip heights, comparing the effects of holding skirt molecules fixed or treating them dynamically. After the system was equilibrated at these positions, the dynamic constraint on skirt molecules was released and the system was allowed to come to a new equilibrium. The skirt was found not to have any significant effect on film structure or dynamics beyond more than one or two molecules away from the frozen ring, and global parameters such as the contact area and tip−wall interaction force were also unaffected, except during unloading at relatively large asperity−surface separations ($h \geq \sim 1.8$ nm). At these heights, where the film was under the largest tensile stress just prior to the rupture of the last few molecular contacts with the planar wall, chains on the upper portion of the tip were more strongly drawn to the frozen skirt than the planar wall, which kept them from reaching down toward the surface. The frozen skirt thus led to fewer atomic contacts with the surface and a smaller overall tensile force during the final stages of contact rupture than those in the same system with all molecules treated dynamically. At smaller tip heights, including the regime of overall repulsive force, the effects of the skirt appeared to be inconsequential. On an actual CFM stylus, chains further up the sides of the tip may play a role similar to that of the confining skirt.

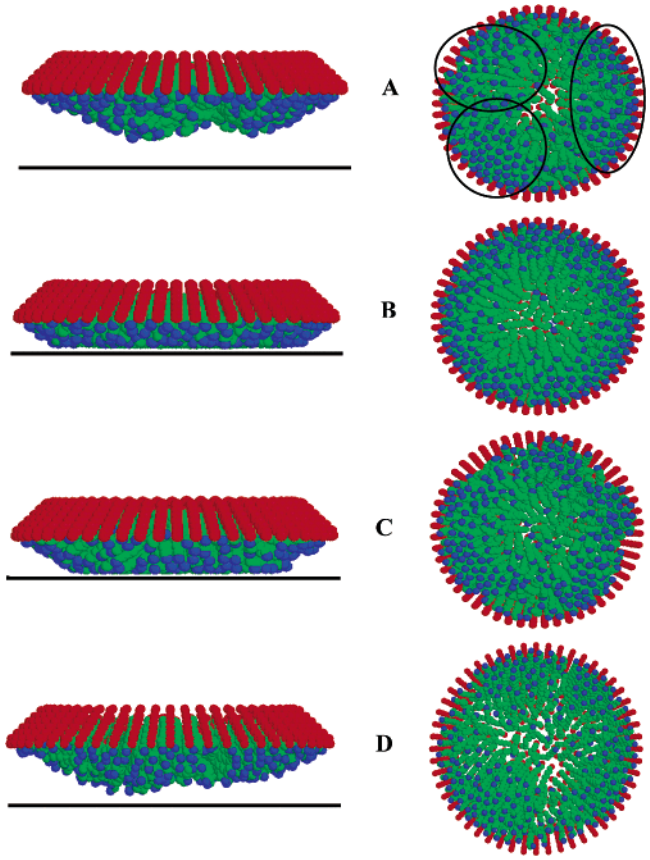

Figure 2. Snapshots of the equilibrated asperity at different heights shown from the side (left) and below (right). Green atoms are methylene, blue atoms are methyl, red atoms are sulfur, and red molecules are part of the frozen skirt. (a) $h = 2.04$ nm prior to approach; (b) $h = 076$ nm, closest approach, largest compressive force; (c) $h = 1.20$ nm unloading, largest tensile force; (d) $h = 2.04$ nm, stylus fully retracted and contact broken.

Results and Discussion

Isolated Stylus. The alkylthiolate film was first characterized through a 0.2 ns simulation carried out with the tip in isolation. By the end of this period, molecules near the frozen skirt had ordered into two or three additional rings; however, beyond this point, further down the tip, the film was less structured, as seen in the snapshot shown in Figure 2A. The sulfur atom lattice was locally hexagonal with a mean interatomic spacing of 0.46 nm. Although the mean area occupied by each sulfur atom differed by less than 1% from comparable alkylthiolate SAMs on planar surfaces, the tip's high curvature resulted in a large excess volume in the outer regions of the film. Consequently, attractive interchain forces led to the formation of small molecular domains or "chain bundles" separated by gaps in the film. Three such domains are identified by circles in Figure 2a. Within each domain, the chains were more or less uniformly tilted and close-packed although less well ordered than those in planar long-chain SAMs at the same temperature.[48] At the borders between domains, the chains were disordered and extended in random directions; a few lay down almost tangentially on the surface of the stylus core. These domain structures were dynamic, gradually changing in shape and position on a time scale of ∼1 ns. They were much smaller than those

(45) (a) Tabor, D.; Winterton, R. H. S. *Nature* **1968**, *219*, 1120. (b) Israelachvili, J. N.; Tabor, D. *Proc. R. Soc. London, Ser. A* **1972**, *331*, 19.
(46) (a) Joyce, S. A.; Houston, J. E. *Rev. Sci. Instrum.* **1991**, *62*, 710. (b) Joyce, S. A.; Houston, J. E.; Michalske, T. A. *Appl. Phys. Lett.* **1992**, *60*, 1175.
(47) (a) Jarvis, S. P.; Oral, A.; Weihs, T. P.; Pethica, J. B. *Rev. Sci. Instrum.* **1993**, *64*, 3515. (b) Jarvis, S. P.; Yamada, H.; Yamamoto, S.-I.; Tokumoto, H. *Rev. Sci. Instrum.* **1996**, *67*, 2281.
(48) (a) Nuzzo, R. G.; Fusco, F. A.; Allara, D. L. *J. Am. Chem. Soc.* **1987**, *109*, 2358. (b) Nuzzo, R. G.; Dubois, L. H.; Allara, D. L. *J. Am. Chem. Soc.* **1990**, *112*, 558.

typically formed by annealed planar SAMs (which can exceed 100 nm in diameter[52]), but comparable in size to those formed on the facets of metal nanoparticles.[30,34]

The film on the isolated stylus differed in several additional respects from SAMs on planar gold surfaces. For example, in contrast to planar SAMs, where close-packing almost entirely blocks access to the substrate, the open volumes at domain boundaries exposed some sulfur atoms, the underlying core sphere, and most especially methylene groups along the chains. Thus, while the chemical properties of planar SAMs are dominated by the terminal functional group, in the stylus SAM, much more of the film's interior was available to participate in chemical interactions. Unlike planar SAM molecules of the same length, which exist almost exclusively in all-trans conformations at room temperature,[48] the simulated film possessed a significant concentration of gauche defects in the torsional angles. In the isolated tip, the overall gauche fraction was 11%, with the most defects occurring in the outermost portion of the film. This is about half the gauche fraction found in MD simulations of dodecylthiolate on 1−2 nm diameter faceted gold clusters at the same temperature[30] but much higher than the fraction in comparable planar SAMs, which have fewer than 1% gauche defects at 300 K.

As mentioned previously, molecules were mobile with chains undergoing lateral motion and rotation around their backbone axis (large-scale diffusive motion was prevented by the sulfur atom tethers). The mean atomic diffusion coefficient of methyl and methylene psuedoatoms was $\sim 1 \times 10^{-7}$ cm^2 sec^{-1}, which is about the same diffusivity as that of lipids in a fluid bilayer membrane.[49] Based on simulations carried out at different temperatures, the film melting point was found to be 263 ± 13 K, approximately 100 K less than the melting point of the corresponding planar SAM. With respect to the concentration and distribution of gauche defects and the degree of overall chain motion, the film on the isolated stylus more closely resembled a planar dodecylthiolate SAM at a temperature of roughly 400 K.[50−52]

Loading−Unloading Sequence. Following equilibration of the isolated stylus, a planar wall was introduced 2.04 nm below the tip core or about 0.5 nm below the film. The wall was then raised at 2 ms^{-1}, pressed against the film, and withdrawn in a simulation of continuous motion. At various tip heights along this trajectory, snapshots were taken and used as starting points for further calculations in which the tip and wall were held fixed and the system simulated until it was brought to equilibrium. Equilibrium was judged to have been reached when global quantities such as the contact force and total potential energy had achieved steady-state values.

The approach−retract sequence was fully reversible with respect to all quantities measured in this study, except at large separations ($h > 1.6$ nm), where hysteresis occurred in some variables. In the hysteretic regime, there existed two structurally dissimilar free energy minima, separated by an energy barrier; one minimum corresponded to a state in which the film stretched out to bring chain ends into contact with the surface, but under tensile stress, and another corresponded to a state in which the film was fully withdrawn onto the asperity, leaving a gap between the tip and surface. Along the unloading branch of the force−separation curve, the system existed in the former state, and during loading, it existed in the latter. The barrier separating the two states existed only over the approximate interval 1.6 nm $\leq h \leq$ 2.04 nm, and outside this regime, the system was essentially fully reversible.

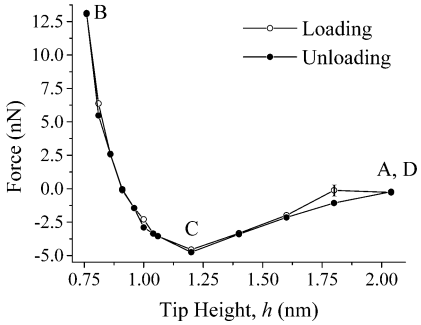

Figure 3. Interaction force between the tip and wall at different stylus heights during both loading and unloading. The labeled points correspond to the same stylus heights represented in Figures 2 and 4. Note the high degree of reversibility at tip heights less than $h \approx 1.6$ nm. The estimated uncertainty in the force is shown for one representative point.

Hysteresis is of course a common occurrence in adhesion, friction, and contact angle measurements, and simulations. Aside from experimental factors such as piezo creep, thermal drift, and so forth,[53] asymmetry with respect to loading and unloading generally results from complicated molecular rearrangements such as interdigitation of molecular chains between contacting surfaces and other nonequilibrium phenomena with long characteristic time scales. In the case of these simulations, nearly complete reversibility may be attributed to the use of long equilibration runs in comparison to the relaxation time of the film following changes in stylus height, which was $\lesssim$1 ns at all tip heights studied. We note that, in a separate study of *continuous* motion with the wall moved at speeds between 1 ms^{-1} and 10 ms^{-1}, hysteresis in the force curve was very pronounced and independent of speed.

Interaction Force. Figure 3 shows the interaction force between the tip and wall as a function of stylus height during loading and unloading. The points which are labeled with letters correspond to the same stylus heights represented by the snapshots shown in Figure 2 and again in Figure 4, discussed below. The first contact between film molecules and the wall occurred at a height of $h \approx 1.8$ nm (the definition of what constitutes contact between film atoms and the wall is discussed later), where, within the resolution of the discretized height data, the contact area changed discontinuously from $A = 0$ nm^2 to $A = 10.2$ nm^2, corresponding to four to six methyl groups in contact with the surface. The onset of repulsion, which corresponds to the inflection point on the loading force curve and is the point where repulsive forces are first detected, occurred at a height of $h = 1.5$ nm. Since this equals the mean thickness of the film measured for the isolated asperity (thickness = 1.53 nm), repulsive forces are seen to develop at the onset of film compression. The corresponding force, known as the contact force, was $F_{\text{contact}} = -3$ nN. The greatest overall attractive force during loading (the *pull-on force*) and unloading (the *pull-off force*) both occurred at $h = 1.2$ nm, with $F_{\text{pull-on}} = F_{\text{pull-off}} =$

(49) Jacobson, K.; Sheets, E. D.; Simson, R. *Science* **1995**, *268*, 1441.
(50) Bhatia, R.; Garrison, B. J. *Langmuir* **1997**, *13*, 765.
(51) Mar, W.; Klein, M. *Langmuir* **1994**, *10*, 188.
(52) Fenter, P.; Eisenberger, P.; Liang, K. S. *Phys. Rev. Lett.* **1993** *70*, 2447.
(53) (a) Staub, R.; Alliata, D.; Nicolini, C. *Rev. Sci. Instrum.* **199**5, *66*, 2513. (b) Hues, S. M.; Draper, C. F.; Lee, K. P.; Colton, R. J. *Rev. Sci. Instrum.* **199**4, *65*, 1561.

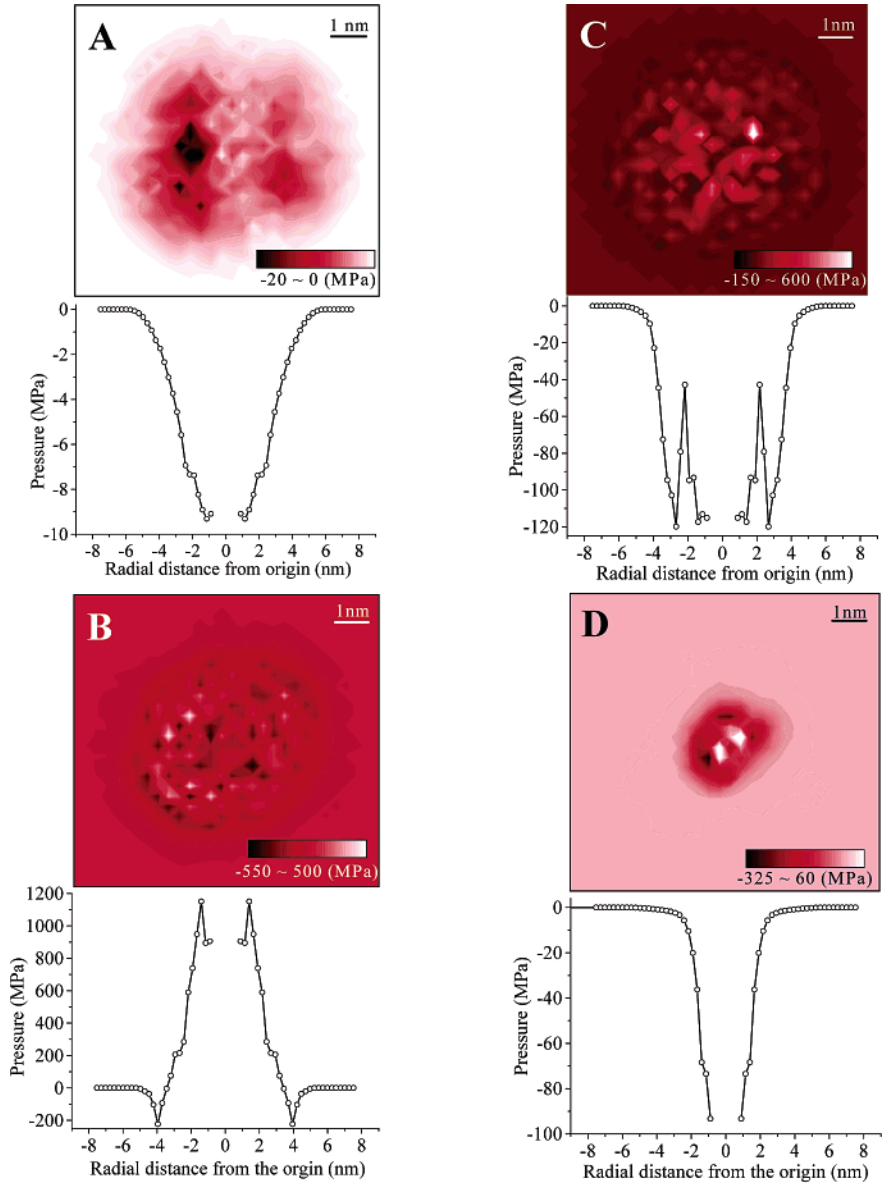

Figure 4. Stress distribution on the planar wall, shown along with its radial average. The stress data were averaged over 1−1.5 ns at each tip height and measured as the normal component of the SAM−wall force per unit area. Negative values correspond to attractive forces. Data at the center of the contact are not plotted because a bald spot developed there in the film, resulting in a low atomic density, which, combined with the small area of the calculation bin, led to large uncertainties in the stress.

−4.8 nN. At this point, the film at the apex was compressed by 20% compared to its relaxed thickness (on the isolated stylus); however, the overall force was dominated by chains further up the sides of the stylus which extended to reach the surface, contributing an attractive force larger than the repulsive force experienced by chains at the apex. Upon further compression, the overall force became repulsive, reaching a maximum value of $F = 13.1$ nN at a tip height of $h = 0.76$ nm.

Some additional details of the interaction force are presented in Figure 4, which shows the stress distribution in the vicinity of the contact zone and its radial average at the same four tip heights labeled by letters A−D in Figure 3. The stress data were averaged over the 1−1.5 ns collection interval at each tip height and measured as the normal component of the SAM−wall force per unit area. Negative values correspond to regions of attractive force. Data at the center of the contact are not plotted because a bald spot developed there in the film, resulting in a low atomic density, which, combined with the small area of the calculation bin, led to unreasonably large uncertainties. The two halves of the radial stress plots at positive and negative radii are perfectly mirrored because they show the same data plotted twice, which was averaged over a complete circle.

The stress distribution is seen to be very uneven and, at small tip heights, subject to large relative fluctuations. These fluctuations are evident in the two-dimensional projections of stress in Figure 4 as closely separated light and dark regions. In some cases, local pressure variations produced pockets of repulsive force adjoining pockets of attractive force with changes of up to 1 GPa over distances less than 1 nm. One such fluctuation was responsible for the anomalous pressure spike in part C at a radius of about 2.0 nm. Also noteworthy is an attractive annulus at the contact perimeter, which existed at even the highest loadings.

Film Structure and Dynamics. When the planar wall first approached the asperity, SAM molecules at the stylus apex extended to reach it, stretching by 15−20% over their mean

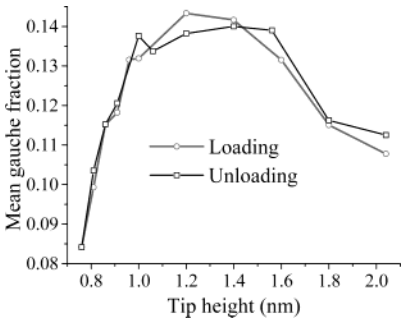

Figure 5. Mean fraction of dihedral angles that were gauche averaged over the entire stylus at each tip height. The gauche fraction for the isolated stylus was much larger than that of a comparable planar SAM at the same temperature. Upon loading, it increased initially due to crumpling of chains at the apex and the creation of a low density region in the film as chains stretched to meet the surface but eventually decreased as the overall force became compressive and chains were forced to adapt more compact conformations.

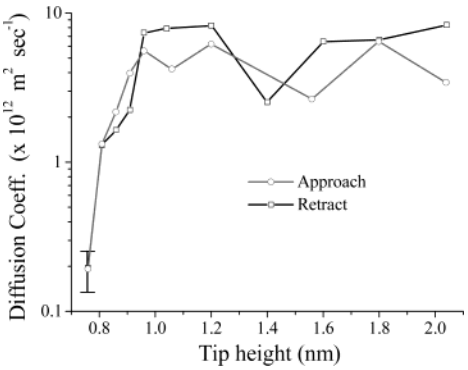

Figure 6. Atomic self-diffusion coefficients averaged over all molecules are shown at each tip height. Because the sulfur atoms were tethered, the long-time displacement averaged to zero, so diffusion coefficients were measured over a limited interval (∼1 ns), where the root-mean-squared displacement increased linearly with time. At $h \approx 1$ nm, chains underwent a compression-induced transition from a fluid to a solid state. The error bars shown for the datum at $h = 0.76$ nm were typical of other points.

relaxed length on the isolated tip. Similar behavior has been observed in models of planar SAMs interacting with a second planar wall or sharp tip, where an increase in tilt angle occurs prior to and immediately after initial contact between approaching surfaces.[26b] In planar SAMs, this results in a initial decrease in the fraction of dihedral bonds that are gauche, which is a convenient measure of conformational order. The gauche fraction at each tip height for the present system is shown in Figure 5. No initial drop was observed; however, this is probably an artifact of the discretized height data, which lacks points in the region immediately prior to contact (i.e., between $h = 1.8$ and 2.04 nm). Figure 5 shows that the gauche fraction first increased to a maximum value of 0.14 and then decreased as the planar wall was further compressed against the film. The overall trend can be explained in terms of the following two factors. First, chains near the tip apex began to crumple almost from the onset of contact with the wall, increasing the number of gauche dihedrals in the affected molecules. The gauche fraction among chains near the apex was actually higher than those elsewhere on the stylus at all heights measured. Second, one consequence of chains at the apex extending to reach the planar wall was the creation of a toroidal volume of depleted chain density in the SAM film immediately surrounding the contact perimeter. Alkylthiolate molecules bordering this low-density region were free to become relatively more disordered than elsewhere on the stylus. As the wall was raised and the film became compressed, the low density region decreased in size until it eventually disappeared altogether at $h \approx 1$ nm. At this point, excluded volume effects began to force improved ordering of the chains on the sides of the tip, leading to a reduction of the gauche fraction, reflecting the need for more compact conformations.

Atomic self-diffusion coefficients were also measured as a function of angular and radial position at each tip height. Because the sulfur atoms were tethered, the long-time displacement averages to zero, so diffusion coefficients were measured over a limited interval (∼1 ns), where the root-mean-squared displacement increased linearly with time. It is worth pointing out that the atomic diffusivity measured here is not the same as the molecular diffusivity reported in some previous studies of planar alkylthiol SAMs.[54] The quantity measured here describes the motion of individual psuedoatoms, whereas the latter describes the motion of the molecular center of mass as thiolates migrate from one Au(111) adsorption site to another. The center of mass diffusivity at room temperature is approximately 10 orders of magnitude slower than the atomic diffusivity measured here, so site-to-site migration would not be observed on the time scale of the simulations even if it weren't restrained from occurring by the sulfur atom tethering potential.

Atoms nearest the ring of frozen molecules encircling the upper portion of the stylus and those in contact with the planar wall were generally least mobile. As shown in Figure 6, the mean diffusion coefficient averaged over all atoms initially fluctuated around $(0.5-1) \times 10^{-11}$ m^2 sec^{-1}. When the wall was raised to $h \approx 1$ nm, the mean diffusion coefficient abruptly decreased, marking the onset of compression-induced film solidification. The height at which this occurred corresponded to the point at which attractive and repulsive forces between the stylus and surface just balanced one another, giving an overall force $F \approx 0$ nN. As mentioned previously, although the total force at $h = 1$ nm was close to zero, there existed large variations in pressure on the planar wall. Attractive forces prevailed around the contact perimeter, but near the center, the pressure averaged ∼1 GPa, and the film thickness at the apex was compressed to about 60% of its relaxed thickness, many atoms having been squeezed out toward the edge of the contact zone. This pressure exceeds the yield strength of bulk gold (∼200 MPa), so some plastic deformation of the end of the stylus might be expected to occur in an actual experiment at the highest loadings. At about the same tip height, the gauche fraction also began to decrease rapidly (Figure 5). By a height of $h \approx 1$ nm, the diffusivity of atoms near the apex was already less than 1×10^{-12} m^2 sec^{-1}, almost an order of magnitude smaller than that of atoms further up the side of the stylus. In fact, at all but the very lowest tip height, atoms on the side of the stylus remained mobile, with diffusion coefficients consistent with a fluid phase. Only at the lowest tip height ($h = 0.76$ nm) did the film become so constrained by the wall below and the frozen ring of molecules above that it solidified everywhere.

(54) (a) Imabayashi, S.; Hobara, D.; Kakiuchi, T. *Langmuir* **2001**, *17*, 2560. (b) Schönenberger, C.; Jorritsma, J.; Sondag-Huethorst, J. A. M.; Fokkink, L. G. J. *J. Phys. Chem.* **1995**, *99*, 3259. (c) Arce, F. T.; Vela, M. E.; Salvarezza, R. C.; Arvia, A. J. *Electrochim. Acta* **1998**, *44*, 1053. (d) Edinger, K.; Golzhäuser, A.; Demota, K.; Wöll, Ch.; Grunze, M. *Langmuir* **1993**, *9*, 4. (e) McDermott, C. A.; McDermott, M. T.; Green, J. B.; Porter, M. D. *J. Phys. Chem.* **1995**, *99*, 13257. Poirier, G. E. *Langmuir* **1997**, *13*, 2019.

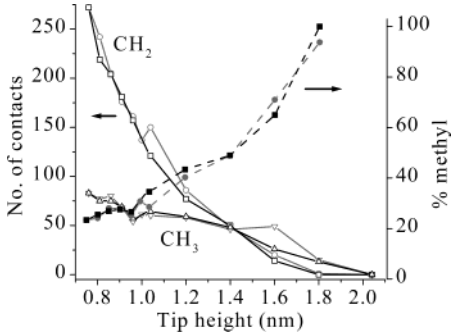

Figure 7. Chemical composition of the contact changed with loading. Plotted against tip height on the left axis are the total number of methyl and methylene psuedoatom contacts and, on the right axis, the percentage of all contacts that were methyl groups. Error bars, calculated as the standard error, were smaller than the size of the data points.

The picture which emerges from these observations is that the film existed in a uniformly fluid state until the height reached about 1 nm. At that point, a set of dramatic changes took place as the gauche fraction and diffusivity began to rapidly decline, and atoms near the apex started to undergo a transition to a solid phase. Some mechanical properties of the film also changed abruptly at this height, as described in the following section. The size of the solidifying region grew as the loading increased, although molecules on the side of the stylus remained fluid until the very lowest tip height. We note that similar compression-induced solidification has been previously observed in simulations of planar SAMs and other fluid systems under loading[26c] and that the findings reported here previously are qualitatively consistent with observations of pressure-induced ordering in alkanethiolate-coated gold nanoparticles.[55]

The chemical composition of the contact also changed during loading. As shown in Figure 7, the fraction of all atomic contacts due to methylene atoms increased steadily as the wall was raised and more of the film's interior was exposed to the planar wall. It is interesting to note that the energy of adhesion, which is the energy required to separate the stylus and wall beginning from the point of zero overall force ($h_o = 0.91$ nm), involves the rupture of 3 times as many methylene−wall bonds as methyl−wall bonds; and, the pull-off force, which is the largest overall attractive force, occurred when approximately two-thirds of all contacts were due to methylene groups. This is counter to the conventional conception that the forces and energies measured by CFM and AFM under conditions of relatively small overall force are due almost entirely to interactions involving only the terminal chain functionality. The distribution was also inhomogeneous within the contact zone, as shown in Figures 8 and 9. Methyl contacts were prevalent at the perimeter, while methylene contacts occurred primarily toward the interior of the contact zone. The relationship between force and contact composition will naturally depend on the details of the chemical interactions involving terminal and film interior groups, but these results serve to highlight the potential importance of the chemistry of the interior of the film and its contribution to adhesion.

An atom was considered to be in contact with the surface if its height was less than or equal to the inflection point in the 12−3 wall potential; that is, if $z \leq (13C_{12}/C_3)^{1/9} + z_0$. For a methyl psuedoatom, this height occurs at $h = 0.39$ nm and lies

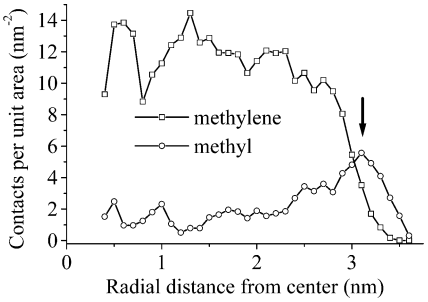

Figure 8. The distribution of surface contacts had a strong radial dependence. The data shown here were collected at $h = 1.2$ nm during unloading and were typical of most points in the simulation. The perimeter was enriched in methyl contacts, while methylene groups accounted for most contacts in the interior. The arrow indicates the radius of the maximum methyl contact density, which was used to compute an alternative measure of contact perimeter (see text).

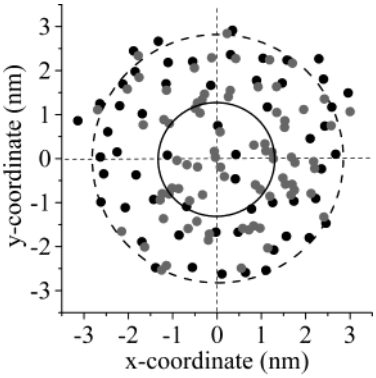

Figure 9. Dots show the distribution of surface contacts at $h = 1.2$ nm during unloading. Black points are methyl contacts; gray points are methylene contacts. The large dashed circle roughly indicates the apparent contact perimeter, as would be determined from a visual inspection. The area enclosed by the inner solid circle was computed from the definition of contact area used in the text.

2.7 *kT* above the minimum in the potential energy well. It was chosen so as to allow an atom undergoing small vertical thermal fluctuations about the minimum to be considered in continuous contact.

Contact Mechanics. In this section, the simulation results are analyzed within the framework of several widely used models of contact mechanics. The most popular of these in the scanning probe microscopy community, and the one which best describes the simulation results, is that due to Johnson, Kendall, and Roberts (the JKR model).[56] The JKR model is derived from the balance of interfacial and elastic distortion energies and is based on the assumptions that the interacting solids are perfectly elastic, the interface is frictionless, and the system remains in thermodynamic equilibrium. Since the flat wall was completely smooth, the assumption of a frictionless contact is satisfied, and all the simulation results pointed to a system at or near equilibrium. It remains to be seen however whether the film responded elastically.

A related model, which is also investigated here, is that of Derjaguin, Muller, and Toporov (the DMT model).[57] The main difference between the JKR and DMT models is the way adhesive forces are treated. The JKR model includes adhesive

(55) Hostetler, M. J.; Stokes, J. J.; Murray, R. W. *Langmuir* **1996**, *12*, 3604.

(56) Johnson, K. L.; Kendall, K.; Roberts, A. D. *Proc. R. Soc. London, Ser. A* **1971**, *324*, 301.

(57) Derjaguin, B. V.; Muller, V. M.; Toporov, P. *J. Colloid Interface Sci*. **1975**, *53*, 314.

forces inside the contact zone but ignores them outside it. It is therefore appropriate for describing contacts with a high adhesion energy, large radius of curvature, and small elastic modulus. The DMT model includes adhesive forces outside the contact zone but ignores them inside it. It is appropriate for contacts involving a weak adhesion, small radius of curvature, and large elastic modulus.

The JKR and DMT models represent limiting cases encompassed by a more general treatment developed by Maugis based on the Dugdale adhesive zone model.[58] In the analysis of this section, the simulation results were fit using the Maugis theory, which enables the most flexible treatment by providing a continuous transition between the two limiting cases described by the JKR and DMT models. The transition between them is governed by the dimensionless parameter λ such that as $\lambda \rightarrow 0$, the equations reduce to those of the DMT model and as $\lambda \rightarrow \infty$, the JKR limit is reached.

The Maugis model involves two equations relating contact radius a and force F:

$$\frac{\lambda \hat{a}^2}{2}\left[\sqrt{m^2-1} + (m^2-2)\cos^{-1}\left(\frac{1}{m}\right)\right] + \frac{4\lambda^2 \hat{a}}{3}\left[\sqrt{m^2-1}\cos^{-1}\left(\frac{1}{m}\right) - m + 1\right] = 1 \quad (1)$$

and

$$\hat{F} = \hat{a}^3 - \lambda \hat{a}^2\left[\sqrt{m^2-1} + m^2\cos^{-1}\left(\frac{1}{m}\right)\right] \quad (2)$$

The variable $m = (d + a)/a$, where d is the distance beyond the contact perimeter where attractive forces cease to act in the Dugdale model. Equations 1 and 2 are written in reduced units, defined as follows:[58]

$$\hat{F} = \frac{F}{\pi W R} \quad (3)$$

$$\hat{a} = a\left(\frac{K}{\pi W R^2}\right)^{1/3} \quad (4)$$

Here, W is the energy of adhesion, and R is the radius of curvature. The reduced modulus K is related to the Young's moduli E and Poisson ratios ν of the stylus and sample by

$$\frac{1}{K} = \frac{3}{4}\left[\left(\frac{1-\nu_{\text{tip}}^2}{E_{\text{tip}}}\right) + \left(\frac{1-\nu_{\text{surface}}^2}{E_{\text{surface}}}\right)\right] \quad (5)$$

In our case, the second term on the right in eq 5 is zero because the surface was perfectly rigid (i.e., $E_{\text{surface}} = \infty$).

To apply these equations, one begins by measuring the contact radius a and force F at a number of different tip heights. Equations 1 and 2 are then solved by iteration to find values for λ and m which simultaneously satisfy (or most nearly satisfy) both equations. This yields a single value for the DMT−JKR transition parameter λ and a set of values for m (a different value for m at each tip height). If R is known from a separate measurement, eqs 3 and 4 can then be used to find the energy of adhesion and reduced modulus. In our case, R is the sum of the tip core radius and relaxed film thickness, $R = 5.00 + 1.53 = 6.53$ nm.

(58) Maugis, D. *J. Colloid Interface Sci.* **1991**, *150*, 243.

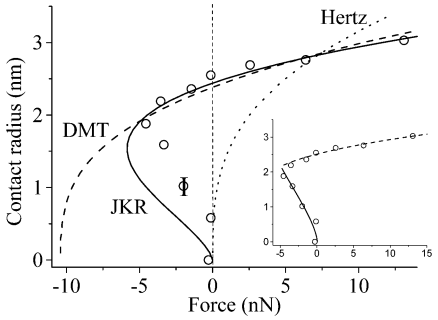

Figure 10. Maugis−Dugdale and Hertz theories were fit to the measured relationship between contact radius and force during unloading. Simulation data are shown as open circles. The estimated uncertainty in the contact radius is shown for one representative point. The best fit in the Maugis−Dugdale theory was found to coincide with the JKR limit and is so labeled in the figure. Also shown for comparison is the best fit in the DMT limit. The inset (which shares units with axes in the main figure) shows the results of dividing the simulation data into two subsets, before and after the point of maximum adhesion, and fitting each subset separately in the JKR limit. The two subsets were fit using a single, fixed value for the work of adhesion, while the reduced modulus was allowed to vary separately. The quality of the resulting fits demonstrates the effect of changing compliance during unloading.

The step which poses the greatest practical difficulty is determination of the contact radius at each tip height. In an actual experiment, a is almost never known but rather must be inferred indirectly from a secondary measurement. Consequently, most authors assume the limiting cases of JKR or DMT mechanics apply in their analysis of AFM, CFM, and related force data, since this leads to closed-form analytical expressions which do not require knowledge of the contact radius. We also present these analyses below as points of comparison.

In this work, the contact area was defined as $A = NA_c$, where N is the number of atomic contacts (methyl + methylene), the area per contact is $A_c = 0.54\pi((1/2)2^{1/6}\sigma)^2$, and σ is the van der Waals size parameter. The factor of 0.54 approximately accounts for overlap between bonded atoms, which reduces the excluded area per atom. The contact zone was assumed (and generally found to be) circular, allowing the contact radius to be computed directly from the area. This definition assumes all atoms occupied the same area when in contact, independent of molecular conformation, pressure, or other influences. It gives a significantly smaller contact area than what might be identified by visual inspection of atomic distributions such as the one shown in Figure 9. In Figure 9, this apparent contact perimeter, indicated by the dashed circle, defines a much larger area than that computed using the previously mentioned formula, which is shown for comparison as the region enclosed by the solid circle. The difference arises because atomic contacts tended to be widely separated, giving a diffuse, mostly empty contact zone. It highlights another important feature of the stylus, surface contact, which is that most of the apparent contact zone actually consisted of empty space. As discussed in the following, some alternative measures of contact area were also considered. However, to within a constant scaling factor, all gave similar results.

The main part of Figure 10 summarizes some results from the Maugis−Dugdale model applied to the unloading branch of the contact radius versus force curve. The best agreement was found to occur when $\lambda \rightarrow \infty$, corresponding to the JKR limit (solid line). Also shown for comparison are the results of fitting in the DMT (dashed line) and Hertz limits (dotted line).

Table 2. Reduced Moduli and Energies of Adhesion in the JKR, DMT, and Hertz Limits[a]

model	adhesion energy, W (mJ m^{-2})	reduced modulus, K (GPa)
JKR	190	11
DMT	250	5
Hertz	N/A[b]	2

[a] Calculated using a tip radius $R = 6.53$ nm. [b] N/A = not applicable.

In the Hertz model, no adhesive forces at all act between the tip and sample.[59] The reduced elastic moduli and energies of adhesion corresponding to these three cases are given in Table 2. The elastic moduli are not dissimilar to those found in previous experimental and computational studies of sharp tips indenting planar alkylthiolate SAMs (5−30 GPa).[26,60,61]

It is apparent from Figure 10 that none of these models provide a particularly accurate description of the simulation data over the whole of the force curve, although the JKR model comes closest to doing so. Among the potential reasons for this poor performance, the contact radius is perhaps deserving of special scrutiny. This is because, even though the positions of all atoms were known, the definition of what constitutes atomic contact between the stylus and surface and, more generally, the way in which the contact radius is defined and measured, are to a certain extent arbitrary, as is inevitably the case when dealing with atomic-sized contacts. Several alternative measures of contact area were therefore also examined but found to be either less reliable or less meaningful than the adopted measure. For example, Figure 8 suggests an alternative definition of contact radius based upon the peak density in the radial distribution of methyl contacts at each height, marked by an arrow. This point may be taken to be related in some way to the contact radius. What is most significant, however, is that all methods considered for measuring the contact radius gave results which were linearly proportional to the adopted measure. The effect in terms of the contact mechanics analysis was therefore only to change the scaling of the ordinate in Figure 10. Alternative measures would therefore have altered the apparent reduced modulus and adhesion energy but would have no impact on the quality of the fit, that is, on the accuracy with which the models describe the simulation results.

We believe there are two factors mostly responsible for the relatively poor performance of the models apparent in the main part of Figure 10. These are their failure to take into account the finite thickness of the compliant layer and the fact that the effective modulus was not constant but instead changed upon loading. As for the former cause, the geometry deviated significantly from the semi-infinite elastic half-space assumed by all the aforementioned models. The effects of this deviation become important when the contact radius approaches or exceeds the thickness of the compliant layer (as was the case over much of the force curve), necessitating finite-size corrections.[62]

The second important contributing factor was the variability of the SAM elastic modulus. The contact mechanics models considered here assume the moduli of all interacting components are unchanging, an assumption which broke down as the SAM underwent a transition from a fluid to a solid under compression below $h \approx 1$ nm. As a consequence of this, none of the models are able to simultaneously fit the contact radius−force profile under both compressive and tensile force regimes due to changes in the film's compliance. The inset in Figure 10 illustrates this point. The data were divided into two parts, above and below the point of largest overall attractive force, and each part fit separately in the JKR limit. Identical values of the stylus radius of curvature ($R = 6.53$ nm) and energy of adhesion ($W = 250$ mJ m^{-2}) were used to fit both parts, while the reduced modulus was allowed to vary freely. The reduced modulus found in the compressive regime (solid line, $K = 13$ GPa) was more than 16 times larger than that found at larger stylus heights (dashed line, $K = 0.8$ GPa), and within each data subset, the fit was very good.

The energy of adhesion W can also be computed directly without assuming a model of contact mechanics by integrating the area under the unloading branch of the force curve from the height of zero force to complete separation and dividing by the contact area at the height of zero force ($\pi a_0^2 = 20.4$ nm^2).[63] Doing so gives $W = 129$ mJ m^{-2}. If one repeats the fitting procedure described previously with the JKR and DMT models but fixes $W = 129$ mJ m^{-2} while allowing K to vary, both models yield poor fits.

It is instructive to compare the results obtained previously for W to those which would be calculated from data provided by an actual experiment, where the contact radius is not directly known. In doing so, we restrict ourselves to the DMT and JKR models, since these models have been used to interpret experimental force measurements in all but a few cases.

In the DMT theory, the contact radius and force decrease smoothly to zero as the tip is withdrawn. In the JKR theory, however, the contact radius jumps discontinuously to zero, the size of the jump depending on the material constants and on whether the stylus and sample positions are rigidly held ("fixed grips") or whether it is the force that is fixed. The simulations modeled a system with fixed grips, and in that case, the contact radius, indentation, and force at the point of separation are predicted to be[58]

$$a_{\text{separation}} = \left(\frac{\pi W R^2}{6K}\right)^{1/3} \quad \text{(JKR theory, fixed grips)} \quad (6a)$$

$$\delta_{\text{separation}} = -\left(\frac{3\pi^2 W^2 R}{4K^1}\right)^{1/3} \quad \text{(JKR theory, fixed grips)} \quad (6b)$$

$$F_{\text{separation}} = -\frac{5}{6}\pi W R \quad \text{(JKR theory, fixed grips)} \quad (6c)$$

$$a_{\text{separation}} = 0,\ \delta_{\text{separation}} = 0, \text{ and } F_{\text{separation}} = -2\pi W R \quad \text{(DMT theory)} \quad (7a-c)$$

$$a_{\text{separation}} = 0,\ \delta_{\text{separation}} = 0, \text{ and } F_{\text{separation}} = 0 \quad \text{(Hertz theory)} \quad (8a-c)$$

In the case of the DMT theory (and Hertz theory, which includes no attractive forces), $F_{\text{separation}}$ is also the point of largest attractive force on the entire force curve. In the JKR theory, under conditions of fixed grips, separation occurs after passing through the minimum on the force curve ($F_{\min} = -3/2\pi WR$),

(59) Hertz, H. In *Miscellaneous Papers*; Macmillan: London, 1896; p 146.
(60) Burns, A. R.; Houston, J. E.; Carpick, R. W.; Michalske, T. A. *Phys. Rev. Lett.* **1999**, *82*, 1181.
(61) Joyce, A.; Thomas, R. C.; Houston, J. E.; Michalske, T. A.; Crooks, R. M. *Phys. Rev. Lett.* **1992**, *68*, 2790.
(62) Shull, K. R. *Mater. Sci. Eng. R* **2002**, *36*, 1.

taking place at *negative* indentation. It should be noted that, in measurements where it is the load, rather than the stylus position that is controlled (such as in AFM where the stylus is part of a flexible cantilever), the JKR expressions differ from those given previously, while the expressions for the DMT and Hertz models are unchanged.[64]

Let us use these expressions to predict the contact radius at separation first. This quantity, along with the separation force, has been used by several authors to estimate "single-molecule" rupture forces. We observe that the various approaches to calculating the adhesion energy and reduced modulus discussed previously gave values in the range $W = 190-250$ mJ m^{-2} and $E = 0.8-13$ GPa. According to the JKR theory then, the separation radius should be 0.73 nm $< a_{\text{separation}} <$ 1.9 nm. The DMT and Hertz theories predict $a_{\text{separation}} = 0$. Within the resolution of the data in Figure 10, the most that can be said is that $a_{\text{separation}} <$ 1.0 nm, which is consistent with all predictions.

If the stylus radius of curvature R is known, the separation force alone can be used to calculate the energy of adhesion using the equations given previously. This was the approach taken for example in ref 65, where the DMT theory was used to help understand measurements performed with the interfacial force microscope. In the case of the simulation results, however, it is clear that inconsistencies between the data and the theory prevent this approach from providing a meaningful analysis. Beginning with the DMT theory, one sees that, according to the equations given previously, the separation force, which is also the point of greatest attraction on the force curve, should occur just as the contact radius reaches zero. As is clear from Figure 10, however, these two forces are very different: $F_{\text{min}} = -4.56$ nN $\neq F_{\text{separation}} \approx 0$ nN. In fact, the points of separation and of greatest attractive force are separated by more than 0.6 nm. In an actual experiment, where the contact radius would not be known, this discrepancy would go undetected. One would normally assume (perhaps incorrectly) that the separation force corresponded to the most attractive point on the force curve and use this point for the calculation of W. Interestingly, if this is done in the present case, one obtains, from eq 7c, $W_{\text{DMT}} =$ 111 mJ m^{-2}, which is close to the value found by direct integration of the force curve (129 mJ m^{-2}).

Applying the JKR theory in an analogous way to compute W using eq 6c presents a different difficulty. If the JKR model is assumed to hold, the point of separation should be identifiable as the position where the force (and contact radius) jumps discontinuously to zero. However, within the resolution of the discretized data, it appears that that the force decreases smoothly to zero, that is, that $F_{\text{separation}} \approx 0$ nN. This result would only be possible within the JKR framework if the adhesion energy was infinitely large.

We should caution that the last 1−2 points on the unloading branch of the force curve (and first 1−2 points on the loading branch) present a special problem, mentioned previously, arising from the bistable character of the free energy surface describing the system in this regime. The barrier separating the two minimum energy states (where one state corresponds to the SAM under tensile stress reaching out to contact the planar wall, and the other, to the SAM fully withdrawn onto the stylus) makes it difficult to accurately locate the point of final separation in a system which may also be mechanically unstable. Obviously, these factors affect any analysis concerning the details of the force curve or contact radius just at the point of rupture. Moreover, these issues are not limited to computer simulations but also occur in real systems, where the thermally activated nature of the transition between bistable states near the point of contact rupture means separation depends not only on the contact mechanics and material properties but also upon the rate at which the contacting parts are separated and the temperature.[66]

Conclusion

In summary, this paper presents results from MD simulations of a sharp stylus covered with a covalently bound alkylthiolate SAM interacting with a smooth, planar wall, along with analysis of the film structure, dynamics, forces, and contact mechanics. The system provides a realistic model of CFM and related techniques performed under conditions of fixed grips and is the first to dynamically model such a system near constant equilibrium.

In the absence of the planar wall, the stylus SAM was found to exist in a fluid state with structural and dynamic properties similar to those of the analogous planar SAM at a somewhat elevated temperature. When the wall was brought into contact with the stylus and pressed against it, a series of reversible changes occurred culminating with solidification of the SAM film at the largest compressive force. During loading, much of the film's interior was exposed to the wall; most of the adhesive force was in fact due to methylene−wall interactions. At all tip heights, the distribution of forces within the contact zone was uneven and subject to large local fluctuations. Analysis using the JKR, DMT, and Hertz contacts mechanics models revealed significant deviations from the simulation results, with the JKR model providing best overall agreement. Some of these discrepancies would be overlooked in an actual experiment, where contact area is not separately known, possibly producing misleading or incorrect results. These shortcomings may be improved upon by using a model that correctly accounts for the finite thickness of the compliant components and nonlinear elastic effects.

Acknowledgment. We would like to thank Malachy Scullion and Nick Ericson for their assistance and for performing preliminary calculations, The Camille and Henry Dreyfus Foundation, and the North American Treaty Organization for supporting this work under NATO Collaborative Research Grant 971003.

JA0345367

(63) The JKR model explicitly separates the elastic and surface energy components (Johnson, K. L. *Contact Mechanics*; Cambridge University Press: Cambridge, 1985), while the energy derived by integrating the force−distance curve includes both contributions. However, the only elastic part in the model comes from stretching of the thiols, which perhaps should be included in the surface energy anyway, since the film is just one molecule thick (as the substrates are rigid and do not interact with one another, they do not contribute any elastic energy).

(64) The contact radius, indentation, and force at the point of separation in the JKR theory under conditions of fixed load are as follows:[58] $a_{\text{separation}} = (3\pi WR^2/2K)^{1/3}$, $\delta_{\text{separation}} = -(\pi^2W^2R/12K^1)^{1/3}$, $F_{\text{separation}} = F_{\text{min}} = -{}^3/_2\pi WR$.

(65) Thomas, R. C.; Houston, J. E.; Crooks, R. M.; Kim, T.; Michalske, T. A. *J. Am. Chem. Soc.* **1995**, *117*, 3830.

(66) (a) Evans, E.; Ritchie, K. *Biophys. J.* **1997**, *72*, 1541. (b) Seifert, U. *Phys. Rev. Lett.* **2000**, *84*, 2750.